Optics Letters

Multi-timescale infrared quantum cascade laser ellipsometry

Andreas Furchner,[1,*] Christoph Kratz,[2] Jörg Rappich,[3] and Karsten Hinrichs[2]

[1]Helmholtz-Zentrum Berlin für Materialien und Energie GmbH, Division of Energy and Information, Schwarzschildstraße 8, 12489 Berlin, Germany
[2]Leibniz-Institut für Analytische Wissenschaften – ISAS – e.V., Schwarzschildstraße 8, 12489 Berlin, Germany
[3]Helmholtz-Zentrum Berlin für Materialien und Energie GmbH, Institut für Silizium-Photovoltaik, Kekuléstraße 5, 12489 Berlin, Germany
*Corresponding author: andreas.furchner@helmholtz-berlin.de

Received 11 March 2022; revised 9 May 2022; accepted 9 May 2022; posted 10 May 2022; published 26 May 2022

We recently introduced a versatile infrared laser ellipsometer for sub-decisecond spectroscopy [Opt. Lett. 44, 4387 (2019)] and 0.03 mm² spot-sized hyperspectral imaging [Opt. Lett. 44, 4893 (2019)]. Here we report on the next device generation for thin-film sensitive simultaneous single-shot amplitude and phase measurements. The multi-timescale ellipsometer achieves 10 µs time resolution and long-term stability over hours at high spectral resolution (0.2 cm⁻¹). We investigate the temporal stages (from minutes to milliseconds) of fatty acid thin-film formation upon solvent evaporation from acetone-diluted microliter droplets. Optical thickness variations, structure modifications, and molecular interactions are probed during the liquid-to-solid phase transition. Multi-timescale ellipsometry could greatly impact fields like *in situ* biosensing, microfluidics, and polymer analytics, but also *operando* applications in membrane research, catalysis, and studies of interface processes and surface reactions.

https://doi.org/10.1364/OL.457688

Infrared (IR) ellipsometry is a well-established nondestructive spectroscopic metrology technique that uses polarized light to probe the optical and physicochemical properties of surfaces and thin films [1–4]. The method measures amplitude and phase information of light upon interaction with a sample, expressed by the ellipsometric angles Ψ and Δ. Structure-sensitive baselines and material-specific vibrational bands in the IR spectral range render IR ellipsometry highly advantageous for analyzing sample properties such as thickness, chemical composition, and molecular interactions.

We recently developed a laser-based IR ellipsometer that overcomes the limitations of classical Fourier-transform-based approaches regarding temporal and spatial resolution. Featuring a broadband-tunable quantum cascade laser (QCL) as brilliant light source and a single-shot four-channel beam-division concept, the instrument enables thin-film-sensitive sub-decisecond spectroscopy [5] and 0.03 mm² spot-sized hyperspectral imaging [6] of ellipsometric amplitudes and phases.

Here, we showcase the next IR laser ellipsometer generation that enables multi-timescale amplitude–phase measurements. Having, with the same instrument, access to different time domains is of high relevance for numerous technology, research, and metrology fields. IR spectroscopic *in situ* and *operando* studies of noncyclic or irreversible processes and reactions—or those restricted by small sample amounts—require short- and long-term measurement prospects, often spanning many orders of magnitude in time. With high-speed electronics readout, flexible polarization optics, and long-term stability, the presented multi-timescale IR QCL ellipsometer satisfies this urgent demand. It unleashes the full potential of IR laser ellipsometry for the analysis of thin films and interfaces by, for the first time, covering wide temporal ranges from 10 µs up to hours at high spectral resolution (0.2 cm⁻¹) and stability (<0.005 in tan Ψ and cos Δ).

The IR laser ellipsometer in our application lab was developed in cooperation with Sentech Instruments GmbH and is depicted schematically in Fig. 1. It comprises an external-cavity QCL (MIRcat-QT-2100, Daylight Solutions), a 50×50 mm² mapping stage, micro-focus lenses for spot sizes of 280×120 µm² (at 65° incidence angle), and beam-division optics (four-faceted gold pyramid) followed by four parallel detection channels. Each channel uses a photovoltaic InAsSb detector (P13894-211, Hamamatsu) and can be fitted with individual polarization optics, such as polarizers (KRS-5 wire-grid, Specac Ltd.) and retarders ($\lambda/4$ at 1666 cm⁻¹, uncoated, Optogama UAB). A set of tandem polarizers in the input arm generates linearly polarized light for probing the sample. Optionally, an insertable achromatic retarder unit [7,8] can generate close-to-ideal circular polarization for measuring properties such as circular dichroism.

The pulsed QCL with adjustable duty cycle of up to 10% is broadband-tunable between 1318 cm⁻¹ and 1764 cm⁻¹ at sweep speeds up to 1500 cm⁻¹/s. Larger ranges are accessible by upgrading the laser with additional (broadband) MIRcat QCL chips. The spectral resolution of 0.2 cm⁻¹ for full-range spectra is well below the one practically reachable with nonlaser-based devices.

An external trigger signal synchronizes the QCL with gated integrators in the detection channels. The detector currents are first converted to voltages using dedicated home-built transimpedance amplifiers. Custom-built boxcar integrators then

Corrected 31 May 2022

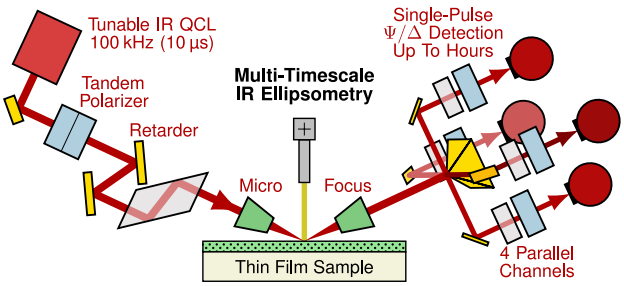

Fig. 1. Schematic of the multi-timescale IR QCL ellipsometer, featuring long-term stable single-shot Ψ and Δ measurements of individual pulses at the laser repetition rate.

average the four intensity signals over each individual laser pulse. Laser repetition rates up to 100 kHz are currently possible.

By simultaneously measuring four polarization states with linearly polarized incident light [5,6], the IR laser ellipsometer can acquire the p- and s-polarized reflectances $|r_p|^2$ and $|r_s|^2$, as well as the ellipsometric ratio

$$\varrho = \tan\Psi \cdot e^{i\Delta} = r_p/r_s \quad (1)$$

in a single shot, that is, for each individual laser pulse, providing both amplitude ($\tan\Psi$) and phase (Δ) information of the sample at the same time. The single-shot scheme significantly reduces environmental influences [9] and allows for stable short- and long-term measurements.

Multi-timescale IR QCL ellipsometry exploits timescales from the 10 µs range, over the sub-second range, up to minutes and hours. In practice, one starts with broadband overview measurements (300–1000 ms). Specific spectral features are then monitored either spectrally (100–300 ms) or, if required in studies of process or reaction kinetics, individually (10–200 µs) by engaging the ellipsometer's high-speed single-wavelength mode.

We applied the laser ellipsometer in a comprehensive multi-timescale study of the formation of thin films of capric acid upon solvent evaporation from acetone/acid microdroplets. For this purpose, gold substrates were covered with rectangular polydimethylsiloxane (PDMS) templates ($4 \times 3\,\text{mm}^2$, 100 µm height) that allow the reproducible placement and defined polarimetric measurement of 3 µl droplets on the sample surface (see Fig. 2).

Time-dependent broadband ellipsometric data of such an experiment are shown in Fig. 3. The process of evaporation and film formation lasts several minutes. However, the actual phase transition takes place on the much shorter millisecond timescale. We divide the process into three stages (exemplary spectra are presented for the ends of stages 1 and 2, and for stage 3).

In stage 1 (after microdroplet placement, not shown), the optical response of the sample is dominated by bulk liquid acetone, which gives rise to dispersion-like acetone vibrational IR bands in $\tan\Psi$ and absorption-like bands in $\cos\Delta$. These spectral features undergo strong shape and baseline changes as the solvent evaporates. In stage 2, after most of the acetone has evaporated, the sample's optical response is that of a thin layer, with absorption-like bands in $\tan\Psi$ and dispersion-like bands $\cos\Delta$. Comparable quantities of fatty acid and acetone are now present within the layer. IR bands of both substances can thus be identified, providing insights into molecular interactions and changes thereof, as is discussed in detail below. In stage 3, the

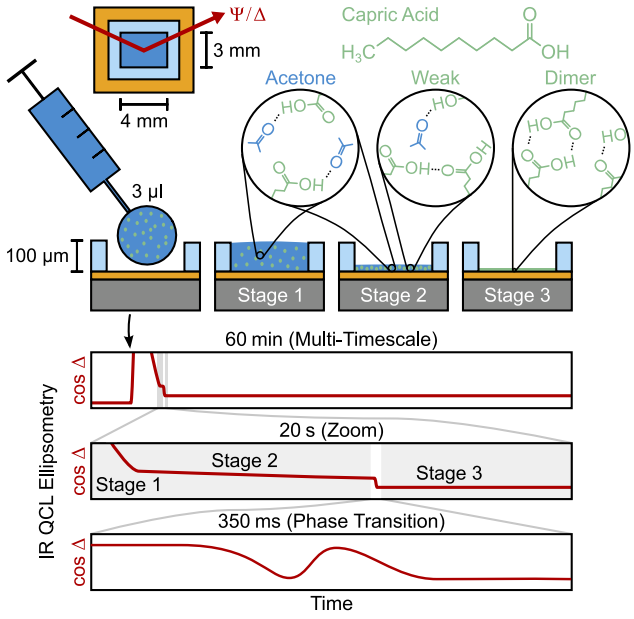

Fig. 2. Measurement scheme of, and changing molecular interactions (acetone-, weakly, and dimer-bound COOH) during, capric acid thin-film formation upon acetone evaporation.

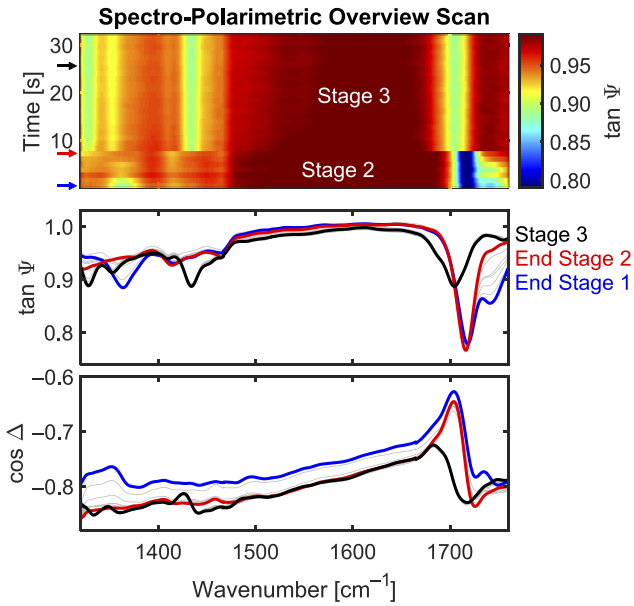

Fig. 3. Overview time-resolved ellipsometric data of the evaporation/film-formation process. Top: hyperspectral visualization. Bottom: spectral representation with exemplary spectra corresponding to the arrows indicated at the top left. In stages 2 and 3, $\tan\Psi$ and $\cos\Delta$ resemble the imaginary (absorption-like) and real (dispersion-like) parts of the thin layer's dielectric function.

acetone has completely evaporated, and a thin film of pure capric acid has formed, as witnessed by distinct changes of the layer's vibrational fingerprint.

In the considered spectral range, acetone, $(CH_3)_2CO$, exhibits two prominent absorption bands at 1712 cm^{-1} and 1362 cm^{-1}, which arise from C=O stretching and CH_3 symmetric deformation modes, respectively [10]. Both bands are visible at the end of stage 1 and the beginning of stage 2, albeit at slightly blueshifted

positions due to optical effects typical for ellipsometric thin-film spectra. As expected, the CH_3-associated band diminishes as the acetone evaporates. The same is true for another broad feature found around 1740 cm^{-1}. However, the strong band observed around 1717 cm^{-1} retains its intensity independent of the layer's acetone content.

The frequency of the C=O stretching mode of fatty acid carboxyl groups depends on the type of intermolecular interaction, that is, whether the COOH groups are acetone-bound, weakly COOH-interacting (termed weakly bound COOH), or exist in the stronger-bound acid dimer form [11,12]. Density functional theory calculations [Gaussian 09, Revision E.01, performed at the B3LYP level of theory using 6-31++G(d,p) basis sets] suggest that the band at 1740 cm^{-1} could be due to C=O stretching of carboxyl groups partially hydrogen-bonded to acetone carbonyl moieties (COOH$\cdots$O=C). This band therefore diminishes upon acetone evaporation. Concomitantly, a redshifted band arises at 1717 cm^{-1} as these COOH moieties now remain only weakly bound to other fatty acid COOH groups. This interplay of changing interactions could explain the observation of a strong and persistent vibrational band at said frequency.

The IR fingerprint of the layer changes drastically as the evaporation process progresses from stage 2 to the acetone-free stage 3. Undisturbed by solvent molecules, the fatty acid's carboxyl groups are now able to self-associate, which can lead to the formation of strong dimeric hydrogen-bond interactions between adjacent COOH groups [13]. These carboxyl dimers exhibit a redshifted C=O stretching mode at about 1704 cm^{-1} as well as an intense in-plane COH bending mode at about 1433 cm^{-1}. Also other bands appear below 1400 cm^{-1} that originate from CH_2 deformations with COOH involvement.

In order to resolve the transitions between the stages, and to capture the details of the observed changes in molecular interactions, we performed additional measurements at a higher time resolution, focusing on the ν(C=O)-associated spectral range. Figure 4 shows a time-dependent polarimetric band scan and exemplary spectra obtained toward the end of stage 1, right at the end of stage 2, and in stage 3 after film formation is complete.

Ellipsometric amplitude and phase data provide complementary insights into the vibrational and structural sample properties. While $\tan\Psi$ is mainly associated with the ν(C=O) band composition, $\cos\Delta$ is an additional measure of the layer's optical thickness ($n \cdot d$) [1]. For instance, pronounced changes in refractive index (n) and thickness (d) are observed in stage 1 as the acetone rapidly evaporates (cf. baselines in Figs. 3 and 4).

The changes in intermolecular interactions and optical thickness can be easily tracked when looking at the ν(C=O) band intensity ($\tan\Psi$) and baseline ($\cos\Delta$) progressions of COOH dimer, weakly bound COOH, and acetone-interacting COOH at 1704 cm^{-1}, 1717 cm^{-1}, and 1740 cm^{-1}, respectively (Fig. 5, top). For stable baselines, lower $\tan\Psi$ values at these wavenumbers correspond to higher band intensity and higher abundance of the respective interacting COOH type. Up until the end of stage 2, there are hardly any $\tan\Psi$ changes in weakly bound COOH groups and in COOH dimers, the latter of which seem to be almost completely absent as long as acetone molecules are still present within the layer. However, as soon as all the acetone has evaporated, previously weakly bound COOH groups seem to immediately turn into COOH dimers (stage 3). The layer's optical thickness, as monitored by $\cos\Delta$, also undergoes a series of changes. Steep drops in $\cos\Delta$ are seen toward the end of

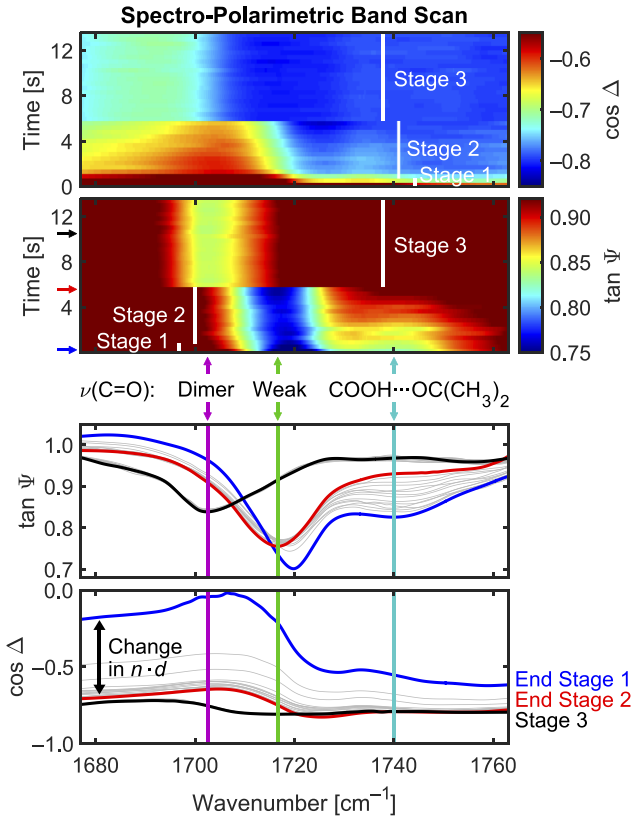

Fig. 4. Time-resolved ellipsometric data of the ν(C=O) region. Top: hyperspectral visualization. Bottom: spectral representation (exemplary spectra corresponding to the indicated arrows, see top left). Vertical lines mark band components associated with acetone-, weakly, and dimer-interacting C=O groups.

stage 1, indicating marked alterations in thickness and/or refractive index due to the quickly evaporating acetone. A further change in optical thickness upon evaporation is evidenced throughout stage 2 by the slight decrease in $\cos\Delta$ at all three wavenumbers, followed by abrupt drops between stages 2 and 3.

Again, the sudden jump from stage 2 to stage 3 is not resolved in the spectral data even with increased time resolution. We therefore further investigated the individual COOH components at sub-millisecond time resolution by making use of the IR ellipsometer's high-speed capabilities. Since dimer formation seems to be triggered only by the presence, or rather absence, of acetone, we focused on the two lower-frequency ν(C=O) bands of weakly (1717 cm^{-1}) and strongly (1704 cm^{-1}) interacting COOH groups. Their band and baseline properties, as measured by $\tan\Psi$ and $\cos\Delta$ at the respective wavenumber, are shown at the bottom of Fig. 5. The phase transition from a mixed layer of fatty acid and acetone to a film of pure capric acid occurs within about 120 ms and is now well resolved by the ellipsometric amplitude–phase measurement.

The sub-millisecond $\tan\Psi$ and $\cos\Delta$ data turn out to exhibit a complex modulation between the two respective vibrational bands. Opposing progressions are observed between the weak COOH and dimer COOH components in amplitude and phase, indicating a simultaneous change in molecular interactions and film structure. In a simplistic model that assumes a direct conversion between two partially overlapping ν(C=O) components, one would expect sigmoidal transitions in both $\tan\Psi$ and $\cos\Delta$.

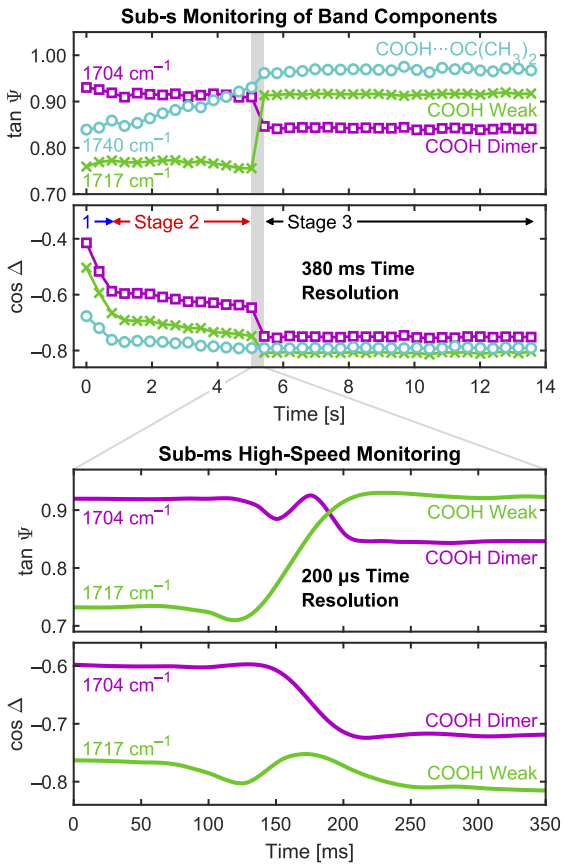

Fig. 5. Time progression of ν(C=O) band components (associated with acetone-, weakly, and dimer-bound COOH) monitored in sub-second spectral and sub-millisecond high-speed mode (at 200 µs time resolution, 5 kHz laser repetition rate).

Over- and undershoots can appear depending on broadening and overlap of the corresponding vibrational oscillators. Additional modulations occur when the thickness and/or refractive index of the layer changes. The latter behavior is indicated by the measured phase data, as $\cos\Delta$ at both wavenumbers exhibits evaporation-induced lower values at the end of the transition than at the beginning.

The sub-millisecond measurements successfully connect ellipsometric amplitude–phase information of the thin film's short-timescale liquid-to-solid phase transition with those of the overall evaporation process that takes place over several minutes.

To conclude, the presented next-generation IR laser ellipsometer for the first time covers multiple timescales separated by orders of magnitude, from minutes/hours down to the 10 µs range. The instrument's single-shot concept significantly reduces environmental influences, allowing stable short- and long-term measurements at 0.2 cm^{-1} spectral resolution. IR laser ellipsometry gives simultaneous access to chemical, structural, and thickness information via the ellipsometric parameters Ψ and Δ. As an application example, we provided comprehensive polarimetric data and interpretation involving the evaporation-induced liquid-to-solid phase transition of fatty acid thin films. Monitoring vibrational bands over long times (10 s to minutes) at high time resolution (sub-millisecond) allowed us to track intermolecular hydrogen-bond interactions involving fatty acid and acetone functional groups. Phase measurements made available by the ellipsometric technique provided additional insights into changes in optical thickness associated with a reduction in layer thickness and a change in refractive index as the solvent evaporates.

This work shows that IR laser ellipsometry enables previously unfeasible *in situ* and *operando* multi-timescale investigations of noncyclic or irreversible processes and reactions at solid–liquid interfaces. In future research, the technique could be applied to study thin-sheet materials used in ultrafast supercapacitors. While the high time resolution will be used for sub-millisecond probing of proton or ion interdiffusion, both short- and long-term monitoring from the sub-millisecond to the hour range are expected to resolve anisotropic effects and structural changes that occur over different timescales. Another potential application is in catalysis and related fields where multi-timescale phase–amplitude monitoring of baselines and absorption bands of catalytic species is expected to yield detailed chemicostructural information on the catalyst. Such investigations will provide a better understanding of short-term catalytic reaction mechanisms and the long-term correlation (even up to days) between catalyst morphology, activity, degradation, and recovery.

Funding. European Regional Development Fund (EFRE 1.8/13); Ministerium für Innovation,Wissenschaft und Forschung des Landes Nordrhein-Westfalen; Die Regierende Bürgermeisterin von Berlin – Senatsverwaltung Wissenschaft, Gesundheit, Pflege und Gleichstellung; Bundesministerium für Bildung und Forschung (CatLab 03EW0015A).

Acknowledgments. The instrument was designed and set up in close collaboration with Sentech Instruments GmbH. We thank U. Richter, G. Dittmar, K. Schreiter, F. Günther, J. Böttcher, M. Hofmann, and J. Reck for support and M. Godejohann (MG Optical Solutions) for advice on laser and boxcar electronics.

Disclosures. The authors declare no conflicts of interest.

Data availability. Data underlying the results presented in this paper are not publicly available at this time but may be obtained from the authors upon reasonable request.

REFERENCES

1. H. G. Tompkins and E. A. Irene, *Handbook of Ellipsometry* (William Andrew, 2005).
2. H. Fujiwara, *Spectroscopic Ellipsometry: Principles and Applications* (John Wiley & Sons, 2007).
3. M. Losurdo and K. Hingerl, *Ellipsometry at the Nanoscale* (Springer, 2013).
4. K. Hinrichs and K.-J. Eichhorn, *Ellipsometry of Functional Organic Surfaces and Films* (Springer-Verlag, 2018).
5. A. Furchner, C. Kratz, and K. Hinrichs, Opt. Lett. **44**, 4387 (2019).
6. A. Furchner, C. Kratz, J. Rappich, and K. Hinrichs, Opt. Lett. **44**, 4893 (2019).
7. J.-C. Cigal, "A novel spectroscopic ellipsometer in the infrared," Ph.D. thesis (Technische Universiteit Eindhoven, 2002).
8. A. Furchner, C. Walder, M. Zellmeier, J. Rappich, and K. Hinrichs, Appl. Opt. **57**, 7895 (2018).
9. K. Hinrichs, T. Shaykhutdinov, C. Kratz, and A. Furchner, J. Vac. Sci. Technol., B: Nanotechnol. Microelectron.: Mater., Process., Meas., Phenom. **37**, 060801 (2019).
10. J.-J. Max and C. Chapados, J. Chem. Phys. **119**, 5632 (2003).
11. C. K. Nandi, M. K. Hazra, and T. Chakraborty, J. Chem. Phys. **123**, 124310 (2005).
12. L. F. L. da Silva, T. Andrade-Filho, P. T. C. Freire, J. M. Filho, J. G. da Silva Filho, G. D. Saraiva, S. G. C. Moreira, and F. F. de Sousa, J. Phys. Chem. A **121**, 4830 (2017).
13. D. Hadži and N. Sheppard, Proc. R. Soc. Lond. A **216**, 247 (1953).